Supporting Information for "Channel-island connectivity affects water exposure time distributions in a coastal river delta"

Matthew Hiatt[1,3], Edward Castañeda-Moya[2,4], Robert Twilley[2], Ben R. Hodges[1], and Paola Passalacqua[1]

[1]Department of Civil, Architectural, and Environmental Engineering, Center for Water and the Environment, University of Texas at Austin, Austin, Texas, USA.

[2]Department of Oceanography and Coastal Sciences, Louisiana State University, Baton Rouge, Louisiana, USA.

[3]Now at: Department of Physical Geography, Faculty of Geosciences, Utrecht University, Utrecht, The Netherlands.

[4]Now at: SE Environmental Research Ctr. & Department of Biological Sciences, Florida International University, Miami, Florida, USA.

Contents of this file

1. Text S1 to S4
2. Figures S1 to S3
3. Table S1

Introduction

The Supplemental Information contains information regarding the determination of the horizontal eddy viscosity for use in the hydrodynamic model (Text S1), a derivation of the equations used to calculate exposure time distributions (text S2), the comparison of the hydrodynamic model with field measurements (Text S3), and the comparison of the mass-flux curves generated by particle tracers versus the advection-diffusion-based tracer (Text S4). The results from the field measurements are included (Table S1).

Text S1 - Determination of horizontal eddy viscosity

The horizontal eddy viscosity, ν_e, can be estimated for shallow flows as [*Cea et al.*, 2007]:

$$\nu_e = \frac{1}{6}\kappa u_\star h \tag{S1}$$

where $\kappa = 0.41$ is the von Karman's constant, $u_\star$ is the bed friction velocity (m s^{-1}), and h is the local water depth (m). The bed friction velocity can be estimated by using the "law of the wall" logarithmic velocity profile:

$$\frac{U}{u_\star} = \frac{1}{\kappa} ln\left(\frac{h}{ez_0}\right) \tag{S2}$$

where U is the depth-averaged velocity (m s^{-1}), e is the base of the natural log, and z_0 is the bed roughness. The bed roughness can be calculated as:

$$z_0 = \frac{aD_{90}}{30} \tag{S3}$$

where $a = 2.85$ is an optimization coefficient and D_{90} is the grain size for which 90% is finer (m) [*Wilcock*, 1996]. Combining Eqs. S1-S3 and using typical velocities within the channel at WLD [*Hiatt and Passalacqua*, 2015] and measurements of D_{90} [*Shaw and Mohrig*, 2014], the horizontal eddy viscosity is $O(0.01 - 0.1)$ m^2 s^{-1}. We select a value of $\nu_e = 0.01$ m^2 s^{-1} for our model simulations.

Text S2 - Derivation of exposure time distribution calculation

Here we provide the full derivation for calculating exposure time distributions in the steady-state case. Some lines are repeated from the main text to maintain the flow of the derivation.

A generic travel time distribution calculated for a system at steady-state can be derived as follows. The differential travel time distribution for a pulse injection at $t = 0$ calculated at the domain boundary at time t is given as [e.g., *Benjamin and Lawler*, 2013]:

$$E(t) = \frac{dN(t)/dt}{N_{Total}} \tag{1}$$

where $dN(t)/dt$ is the rate at which material exits the domain at time t and N_{Total} is the cumulative amount of material that has passed through the system at $t = \infty$. Integrating over time gives the cumulative travel time distribution:

$$F(t) = \int_0^t E(\tau) d\tau \tag{2}$$

where τ is a dummy variable and $F(t = \infty) = 1$, rendering $E(t)$ and $F(t)$ a probability density function (pdf) and cumulative distribution function (cdf) of the travel time distribution, respectively.

In a discrete case, the mass (or particle) flowrate of tracer per unit length at any location along the exit boundary of the system is given as:

$$\frac{dm(x_B,t)}{dt} = u_\perp(x_B,t)\cdot c(x_B,t)\cdot H(x_B,t). \tag{3}$$

where m is the mass per unit length ($kg\ m^{-1}$), $u_\perp$ is the component of velocity perpendicular to the plane of interest ($m\ s^{-1}$), c is the concentration of tracer ($kg\ m^{-3}$), x_B is the system boundary coordinate, and H is the water depth (m). Defining the volumetric flowrate of water per unit length as $q_\perp = u_\perp H$ and integrating spatially over the domain boundary gives the mass flowrate of tracer exiting the system at time t:

$$\frac{dN(t)}{dt} = \int_{x_{b,0}}^{x_{b,n}} \frac{dm(x_B,t)}{dt} dx_B = \int_{x_{b,0}}^{x_{b,n}} q_\perp(x_B,t)\cdot c(x_B,t)\, dx_B \tag{4}$$

The cumulative mass of tracer that exits the system a $t=\infty$ is thus:

$$N_\infty = \int_0^\infty \int_{x_{b,0}}^{x_{b,n}} q_\perp(x_B,\tau)\cdot c(x_B,\tau)\, dx_B\, d\tau \tag{5}$$

where N_∞ is also equal to the initial mass of tracer released for a pulse input with no return flow. Substituting Eqs. 4 & 5 into Eq. 1 yields the differential travel time distribution:

$$E(t) = \frac{\int_{x_{b,0}}^{x_{b,n}} q_\perp(x_B,t)\cdot c(x_B,t)\, dx_B}{\int_0^\infty \int_{x_{b,0}}^{x_{b,n}} q_\perp(x_B,\tau)\cdot c(x_B,\tau)\, dx_B\, d\tau} \tag{6}$$

Eq. 6 is solved discretely at the domain boundary at each time step for model runs without return flows.

The mass flux of tracer at any transect within the domain can also be calculated following a formulation similar to that of Eq. 6. Following the derivation of Eq. 6, the fractional mass flux $e_i(t)$ at any transect x_i is given as:

$$e_i(t) = \frac{\int_{x_{i,0}}^{x_{i,n}} q_\perp(x_i,t)\cdot c(x_i,t)\,dx_i}{\int_0^\infty \int_{x_b,0}^{x_{b,n}} q_\perp(x_B,\tau)\cdot c(x_B,\tau)\,dx_B\,d\tau} \quad (7)$$

Note that the denominator of Eq. 7 is the same as that of Eq. 6, which renders $e_i(t)$ a local breakthrough curve normalized by the total amount of tracer exiting the system domain.

Text S3 - Hydrodynamic model assessment

The Frehd model was assessed by comparing to calculated discharges from ADCP transects collected in the major distributary channels at WLD. The velocity transects comprised a range of tidal conditions from comparison. A summary of the results from each field trip is contained in Table S1.

Discharge was measured by traversing transects in the major WLD distributary channels (Figure S1 - Locations Apex, A, B, C, D, E, CL, and CR) with a 600 kHz Teledyne RD Instruments Workhorse Rio Grande Acoustic Doppler Current Profiler (ADCP) in conjunction with differential GPS. The ADCP was mounted to the *R/V Lake Itasca* and sat 0.4 m below the water surface.The bin size was set to 0.50 m, the blanking distance was 0.44 m, and the boat speed was maintained at less than 1.0 m s^{-1}. The velocity transects were measured on 15 February 2013 from 08:00 to 12:00 and from 12:00 to 16:00 CDT in an attempt to capture the falling and rising tides, respectively. The measurements coincided with a steady seasonal hydrograph at the USGS gage at Calumet, LA on the WLO. Flows had been near 1000 m^3 s^{-1} for much of the winter before rising and topping 4200 m^3 s^{-1} by 1 February 2013. On 15 February 2013, the station recorded a maximum flowrate of 4530 m^3 s^{-1} and a minimum of 3850 m^3 s^{-1}. For each cross section, two consecutive passes (right bank to left bank, then left bank to right bank) at each transect location were conducted during the predicted falling and rising tides. The field trip was conducted during a neap tide with relatively high river discharge.

In June 2014, discharge was again measured in the major distributary channels at WLD (Figure 1a - Locations A', B, C, D, E, and F). Coinciding with predictions for the spring and neap tides, velocity transects were sailed on 15 June 2014 and 20 June 2014, respectively. The ADCP measurement set up coincides with the methods of *Hiatt and Passalacqua* [2015]. We measured velocity profiles along the transects with the 2 MHz RDI StreamPro with the long-range upgrade measuring in water mode 12sp. Due to depth limitations associated with the ADCP, transects Apex and A could not be measured since they were greater than seven meters in depth. The ADCP was floated alongside the bow of the *R/V Bluerunner* and the transect was traversed four times at an average boat speed of about 1.0 m s^{-1}. The data output rate was maintained at 1 Hz and each collected velocity ping was averaged from eight subpings. The ADCP transducer was $0.15 - 0.20$ m below the water surface, depending on channel depth and surface roughness conditions. The blanking distance was 0.27 m. Depth profiles were linearly extrapolated to the channel banks at a distance estimated from satellite imagery. ADCP transects were collected during both rising and falling tides. The flow entering the WLD at transect A was 2880 m^3 s^{-1} during falling tide on 20 June 2014 and the average from the Calumet gage was about 3450 m^3 s^{-1} [*USGS*, 2016]. To calculate discharge for both field trips, the measured velocities were projected onto the average flow direction for each transect. Teledyne RDI's WinRiver II software was used to process the GPS and ADCP data and output water discharge within each cross section. The average measured discharge through the apex of WLD was 3300 m^3 s^{-1}.

The discharges measured in the field are normalized for comparison with the modeled discharges. The normalized transect discharge ($\hat{Q}$) is obtained by dividing the transect discharge Q by the discharge entering WLD through the Apex transect. Since, the Apex discharge was not measured during the June 2014 field trip, the sum of discharges passing through B, C, D, E, and F was used for normalization. This assumption is reasonable considering the good agreement obtained among the measurements at A', B, C, D, and E on 20 June (ratio = 1.03). The modeled flow partitioning is compared to the field discharge results in Fig. S2 for the river-only and tidal cases during spring and neap tide.

In general, $\hat{Q}$ does not significantly vary for each transect across the model results and field observations. The average variability among the measurements at each transect is 5% and the maximum variability occurs at transects A and D (8%). Transect D consistently receives the largest allocation of flow among the major bifurcates downstream of the Apex and transect A. Transect C receives about 25% of the total flow through the system followed by B, E, and F. A large flow asymmetry exists at the CR-CL bifurcation, with CL receiving the majority of flow from transect C. The cross-sectional area is a good predictor of discharge (Table 1), which agrees well with the control of depth on bifurcation flow asymmetry.

Text S4 - Particle tracer breakthrough curves compared to advection diffusion tracer

As discussed in the main text, we use a particle tracking code to determine ETD over many model runs and at each grid cell within the domain of interest. The particle tracking code reduces the computational effort that would be required to do so with the diffusive tracer. We compare the mass flux distributions from both the particle tracking and advection-diffusion tracers for the WLD model runs. Both the particles and the passive tracer are released at the delta apex. The particle tracer mass flux curves compare well to those generated with the diffusive tracer (Fig. S3). A Wilcoxon rank-sum test was performed to test the statistical similarity of the breakthrough curves generated by the diffusive tracer and the particle tracking. The null hypothesis of equivalent distributions was not rejected at the 5% significance level for the river-only ($p = 0.28$), the spring tide ($p = 0.89$), and the neap tide ($p = 0.65$) model runs. Therefore, the particle tracers are a sufficient representation of the transport within the system.

References

Benjamin, M., and D. Lawler (2013), *Water Quality Engineering*, 1st ed., Wiley, Hoboken, NJ.

Cea, L., J. Puertas, and M.-E. Vázquez-Cendón (2007), Depth averaged modelling of turbulent shallow water flow with wet-dry fronts, *Archives of Computational Methods in Engineering*, *14*(3), 303–341, doi:10.1007/s11831-007-9009-3.

Hiatt, M., and P. Passalacqua (2015), Hydrological connectivity in river deltas: The first-order importance of channel-island exchange, *Water Resour. Res.*, *51*, 2264–2282, doi:10.1002/2014WR016149.

Shaw, J., and D. Mohrig (2014), The importance of erosion in distributary channel network growth, Wax Lake Delta, Louisiana, USA, *Geology*, *42*, 31–34, doi:10.1130/G34751.1.

USGS (2016), U.S. Geological Survey (USGS) water data for the nation, available online at http://waterdata.usgs.gov/nwis/ (last accessed February 20, 2016).

Wilcock, P. R. (1996), Estimating local bed shear stress from velocity observations, *Water Resour. Res.*, *32*(11), 3361–3366, doi:10.1029/96WR02277.

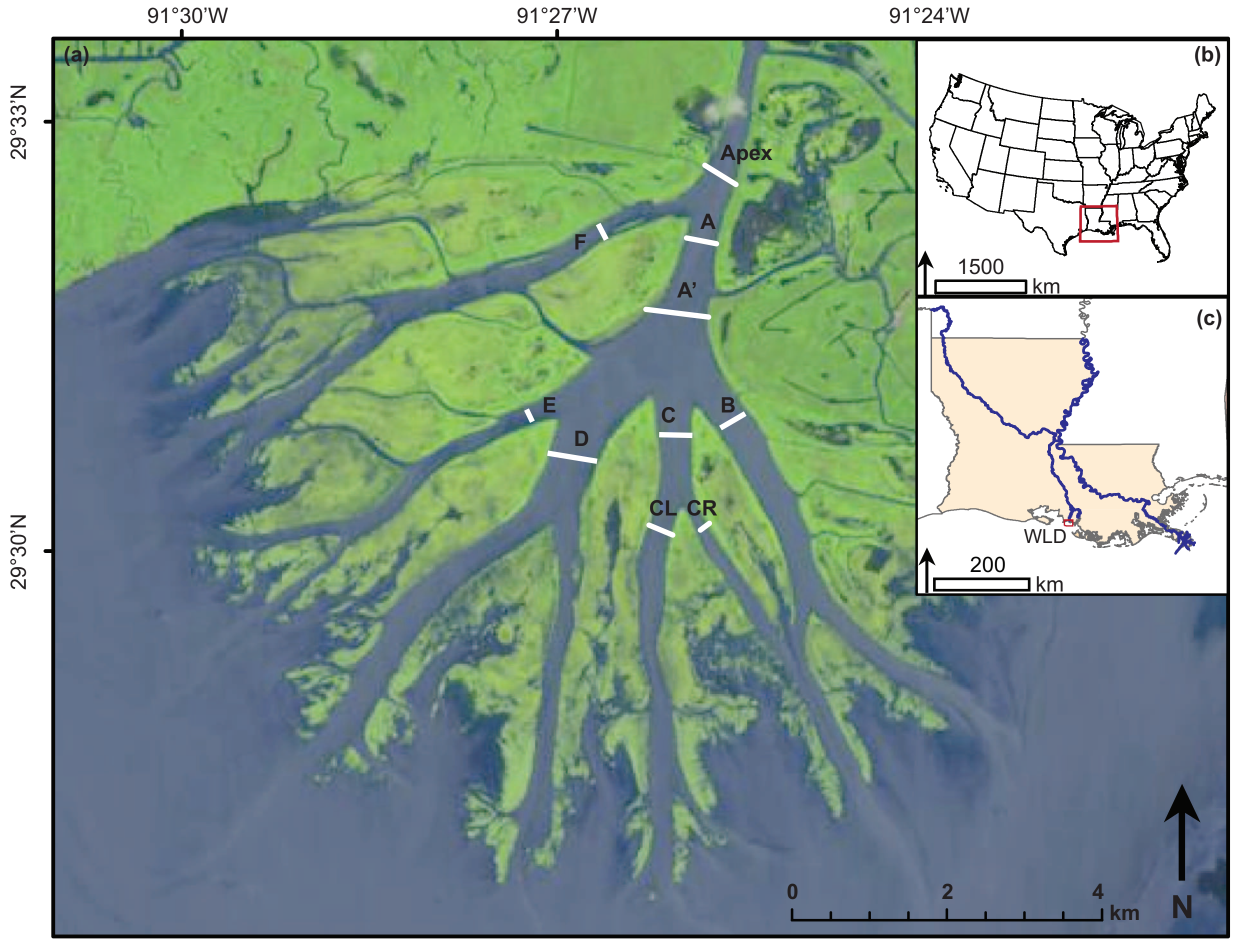

Supplementary Figure 1. Map of Wax Lake delta (WLD). Locations of acoustic Doppler current profiler transects. (b) The location of Louisiana on a United States map. (c) Map of major river systems in Louisiana and the location of WLD.

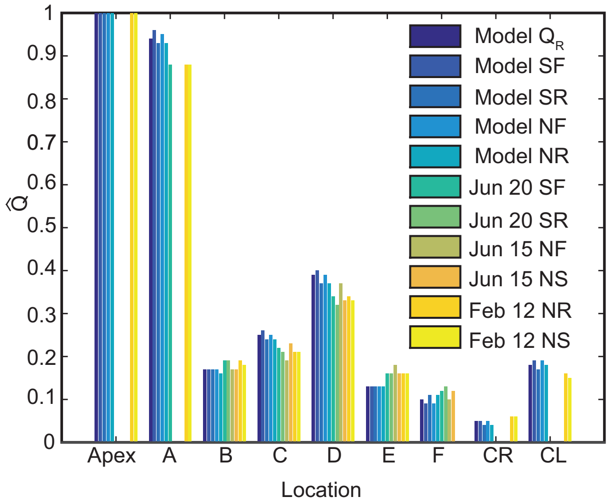

Supplementary Figure 2. Assessment of the hydrodynamic model on the WLD domain. The fractional discharge ($\hat{Q}$) is compared among the various model runs and field data sets. The model is not calibrated to the field results, but provides good qualitative agreement with the actual flow partitioning at WLD.

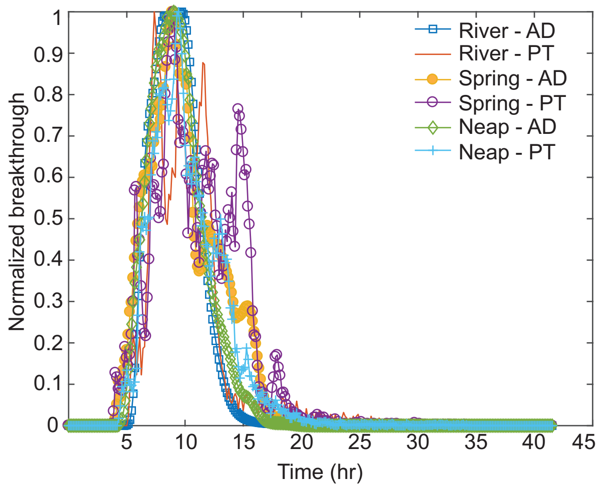

Supplementary Figure 3. Comparisons among the breakthrough curves for the diffusive tracer (denoted AD in figure) and the particle tracers (PT). In each scenario, the distributions for the AD and the PT are statistically similar according to a Wilcoxon rank-sum test at the 5% significance level (p-values: 0.28, 0.89, and 0.65 for river, spring, and neap, respectively).

Supplementary Table 1. Average discharge, area, and width measured by the ADCP on 15 February 2013 and 15 and 20 June 2014. Transects averaged over fewer than four repeat measurements are italicized for the June 2014 field trip.

Time and Date	Location	Tide	Q (m^3 s^{-1})	Area (m^2)	Width (m)
08:02 15 Feb	Apex	Fall	3734 (26)	3951 (49)	437 (61)
08:23 15 Feb	A	Fall	3278 (14)	3696 (11)	396 (1)
08:47 15 Feb	E	Fall	588 (4)	935 (5)	289 (3)
09:08 15 Feb	D	Fall	1279 (7)	2209 (11)	682 (4)
09:46 15 Feb	C	Fall	796 (12)	1244 (7)	428 (2)
10:13 15 Feb	B	Fall	681 (5)	1189 (20)	493 (7)
10:39 15 Feb	CR	Fall	221 (25)	397 (30)	160 (15)
10:54 15 Feb	CL	Fall	572 (1)	940 (23)	309 (6)
12:31 15 Feb	CL	Rise	582 (3)	950 (5)	309 (4)
12:49 15 Feb	CR	Rise	228 (14)	420 (31)	176 (17)
13:38 15 Feb	B	Rise	683 (18)	1248 (1)	523 (4)
13:59 15 Feb	C	Rise	775 (5)	1275 (14)	439 (3)
14:26 15 Feb	D	Rise	1250 (5)	2254 (2)	682 (4)
14:53 15 Feb	E	Rise	580 (3)	926 (1)	285 (3)
15:19 15 Feb	A	Rise	3225 (33)	3755 (18)	411 (19)
15:41 15 Feb	Apex	Rise	3671 (38)	3851 (12)	378 (9)
08:45 15 Jun	B	Fall	*430* (5)	*1266* (91)	*490* (16)
09:18 15 Jun	C	Fall	466 (24)	1309 (128)	455 (42)
10:22 15 Jun	F	Fall	247 (26)	868 (26)	301 (14)
10:59 15 Jun	E	Fall	447 (10)	913 (18)	310 (8)
11:38 15 Jun	D	Fall	*914* (5)	*2230* (147)	*668* (36)
13:16 15 Jun	B	Lower-high	468 (8)	1153 (58)	466 (18)
14:02 15 Jun	C	Lower-high	*625* (18)	*1217* (28)	*423* (8)
14:58 15 Jun	D	Lower-high	880 (74)	2095 (32)	653 (17)
16:06 15 Jun	E	Lower-high	418 (18)	888 (33)	309 (8)
16:53 15 Jun	F	Lower-high	317 (22)	804 (14)	293 (3)
08:52 20 Jun	D	Rise	971 (10)	2161 (27)	640 (6)
09:50 20 Jun	E	Rise	448 (7)	870 (29)	314 (28)
10:29 20 Jun	C	Rise	610 (3)	1274 (18)	465 (9)
11:13 20 Jun	B	High	537 (6)	1198 (22)	501 (7)
12:43 20 Jun	F	Fall	364 (4)	802 (17)	306 (3)
13:25 20 Jun	D	Fall	1118 (14)	2208 (33)	699 (20)
14:11 20 Jun	E	Fall	530 (9)	867 (12)	324 (7)
14:40 20 Jun	A’	Fall	*2899* (10)	*4359* (214)	*928* (8)
15:32 20 Jun	C	Fall	716 (10)	1195 (15)	449 (9)
16:32 20 Jun	B	Fall	619 (9)	1122 (20)	502 (6)
17:11 20 Jun	F	Fall	381 (9)	728 (20)	296 (6)